Journal of Electronics and Information Science (2024)
Clausius Scientific Press, Canada

DOI: 10.23977/jeis.2024.090113
ISSN 2371-9524 Vol. 9 Num. 1

Communication and sensing performance study of NOMA-ISAC system with IRS-assisted SWIPT

Dongkai Cui[a,*], Ya Li[b], Kailuo Zhang[c], Xin Wang[d]

School of Physics and Electronic Information, Henan Polytechnic University, Jiaozuo, 454003, China

[a]212111020009@home.hpu.edu.cn, [b]liya@hpu.edu.cn, [c]756620696@qq.com, [d]239777081@qq.com

[*]Corresponding author

Keywords: Integrated sensing and communications, non-orthogonal multiple access, intelligent reflecting surface, simultaneous wireless information and power transfer

Abstract: Integrated sensing and communication (ISAC) and non-orthogonal multiple access (NOMA) are critical technologies for beyond 5th generation (B5G) and 6th generation mobile communications owing to their exceptional spectral efficiency and efficient hardware resource utilization. These technologies are widely utilized in emerging industries such as intelligent transportation systems for smart cars. Based on this, this paper explores a single-lane scenario using a NOMA-ISAC network, complemented by the assistance of an intelligent reflecting surface (IRS) and simultaneous wireless information and power transfer (SWIPT). The purpose of this investigation is to jointly evaluate the performance of both radar and communication functions. That is, the base station (BS), the detection vehicle (Alice), and the target vehicle (Bob) form a NOMA-ISAC network, the network can achieve both energy harvesting with the assistance of an IRS, and sensing of Bob by Alice. In particular, an energy harvesting strategy with time switching is used to implement energy supply from BS to Alice. Closed-form expressions are derived to evaluate the outage probability (OP) for Alice and Bob. The probability of detection (PD) and joint detection communication coverage probability (JDCCP) at Alice is also analyzed.

1. Introduction

The sixth generation (6G) mobile communication technology will empower the interconnection of everything from things to things, things to people, and people to people, that is, "Internet of Everything and Digital Twin". Emerging applications such as smart cars and unmanned aerial vehicles (UAVs) will have an increasing demand for systems that combine both communication and radar sensing capabilities[1]. On the other hand, with the continuous development of hardware and software, the bandwidths of radar sensing and wireless communication technologies are gradually overlapping[2]. Integrated sensing and communication (ISAC) offers a new approach to designing and modeling new network architectures and protocols that can benefit from the synergy of communication and radar systems[3].

ISAC integrates both communication and sensing functions, which can sense channel characteristics, interference conditions and other conditions in the network in real time and make

corresponding adjustments, thus improving communication reliability and stability[4]. On the other hand, ISAC can effectively manage resources and energy, and achieve the need of quality of service by dynamically allocating and scheduling resources[5]. Authors in [6] proposed a deep learning-based approach for accurate sensing-assisted beam tracking in high-mobility vehicle networks, which estimated angular parameters of vehicles based on radar echoes to perform predictive beamforming with high accuracy and low latency, improving estimation performance and maintaining reliable communications. Wang et al. in [7] proposed a joint waveform and discrete phase shift design using reconfigurable intelligent surfaces to mitigate multi-user interference in ISAC systems under Cramer-Rao bound constraint. In [8], the authors investigated a NOMA-enhanced ISAC framework which achieved the optimization of both communication throughput and target sensing effects by optimizing the beamforming design. And the numerical results verified that NOMA-ISAC could exhibit better performance than the conventional integrated sensing and communication framework under highly correlated channel underload and overload conditions.

To enable information transmission in ISAC networks with limited spectrum resources, NOMA technology is an excellent choice, as successive interference cancellation (SIC) technology is well suited to the ISAC scenario[9]. Firstly, NOMA can serve multiple devices simultaneously and provide a relatively balanced service while ensuring the QoS required by the devices [10]; furthermore, because the SIC scheme has been well researched, we have a strong basis to implement decoding of sensed and communicated signals at the receiving end [11]. In [12], the authors proposed a novel ISAC with iterative channel estimation method which allowed multi-channel estimation from received communication and sensing signals to provide spectral efficiency while maintaining sensing and communication performance, which enables NOMA with linearithmic complexity. In [13], the authors analyzed the performance of an uplink ISAC system, where the communication phase used the NOMA protocol. The outage probability (OP), the ergodic communication rate and the sensing rate were also derived, and the results showed that the sensing rate of the ISAC system is higher than that of the frequency-division sensing and communications system for the same communication rate.

However, communication nodes and sensing nodes are usually limited by the amount of energy stored in the battery due to mobility or other limitations [14]. To extend life, simultaneous wireless information and power transfer (SWIPT) is considered as a promising method. We envision a future 6G network with integrated NOMA-ISAC that will enable a new multifunctional wireless system for sensing, communication and energy transmission simultaneously. This versatile wireless system is expected to significantly improve the utilization efficiency of scarce spectrum resources and densely deployed BS infrastructure, as well as facilitate the localization and power of large-scale low-power devices to support emerging IoT applications [15]. Xia et al. in [16] proposed an online optimization algorithm for energy harvesting-based mobile edge computing systems. The online optimization algorithm used game theory and regenerative Lyapunov optimization theory to manage task offloading, computational resource allocation, and battery energy. Authors in [17] provided a comprehensive performance evaluation of UAV relay networks employing NOMA technique, and considered a cooperative communication where a wirelessly-powered UAV was served as a mobile relay and deriving closed-form expressions of OP and ER for both amplify-and-forward and decode-and-forward relaying protocols with extensive simulations verifying the accuracy of the derived expressions.

Although energy harvesting can achieve energy transmission through radio frequency signals, which improves the convenience and flexibility of node devices, its transmission distance and transmission efficiency are somewhat limited [18]. Combining energy harvesting and intelligent reflective surface (IRS) can further improve the efficiency and flexibility of energy transmission[19]. Liu et al. in [20] proposed a proximal policy optimization based transmit

beamforming and phase-shift design for an IRS-aided ISAC system in the terahertz band. The proposed method optimizes the sum rate of the system while satisfying the power constraint at the transmitter and the signal-to-interference-plus-noise ratio (SINR) requirement at the receiver. In [21], the authors analyzed the performance of IRS-assisted NOMA networks with randomly deployed users. The paper investigated the OP and ER of the system in different scenarios, including single-user and multi-user channels. Numerical results show that the proposed IRS-assisted NOMA scheme significantly improves the system's performance compared to conventional schemes. Authors in [22] proposed an IRS-assisted downlink and uplink NOMA scheme for wireless powered communication networks and provides efficient algorithms to optimize reflection coefficients, beamforming vectors, and resource allocation for maximizing uplink sum-rate while ensuring the minimum rate requirement at information receiving devices.

2. System Model

2.1. Network Model

As shown in Figure 1, we consider a single-lane scenario for a downlink, where the entire network consists of a BS, a roadside setup unit (RSU) equipped with an IRS with K elements, and two NOMA users (the near user Alice and the far user Bob), where Alice is the detector and Bob is the sensing target. Specifically, Alice transmits a sensing signal to the front-end after receiving the energy supply reflected from the BS and the IRS, while the BS communicates to both Alice and Bob through the IRS and the direct link.

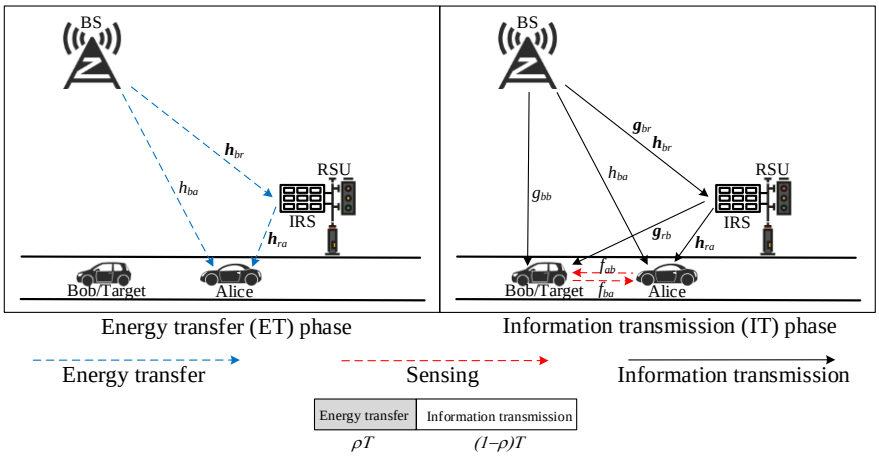

Figure 1: NOMA-ISAC system model with IRS-assisted SWIPT.

In this study, we have the following assumptions: 1) Due to the deployment-friendly nature of IRS, we divide the K elements into two subsets, i.e., K_n elements serving Alice and K_m elements serving Bob; 2) All nodes except Alice and RSU are equipped with a single antenna; 3) Alice operates in full duplex mode and can use a number of advanced residual self-interference cancellation techniques to achieve high quality self-interference suppression. 4) All channels undergo a Rayleigh Rayleigh fading, denoted as $h_{br} \sim CN\left(0, \lambda_{br} I_{K_n}\right)$, $h_{ra} \sim CN\left(0, \lambda_{ra} I_{K_n}\right)$, $h_{ba} \sim CN\left(0, \lambda_{hba}\right)$, $g_{br} \sim CN\left(0, \lambda_{br} I_{K_m}\right)$, $g_{rb} \sim CN\left(0, \lambda_{rb} I_{K_m}\right)$, $g_{bb} \sim CN\left(0, \lambda_{gbb}\right)$, $f_{ab} \sim CN\left(0, \lambda_{ab}\right)$, $f_{ba} \sim CN\left(0, \lambda_{ba}\right)$.

2.2. Signal Model

BS uses a time-switching (TS) strategy for Alice's energy supply, i.e., it is divided into energy transfer (ET) and information transmission (IT) phases in a single time period. In addition to this, we assume that the conversion efficiency, the time switching factor, and the total time of each frame transmission are known \cite{111}.

2.2.1. EH phase

The BS transmits the radio frequency (RF) energy to Alice in the ET phase through the direct link and IRS for a duration of ρ T, where ρ is the time switching factor and T is the total time of each transmitted frame. Thus the energy obtained by Alice in the ET phase can be expressed as

$$E_A = P_{BS}\eta\rho T\left|h_{ra}\Theta_A h_{br} + h_{ba}\right|^2 \tag{1}$$

where P_{BS} is the transmit power at BS, and ρ is the energy conversion efficiency. $\Theta_A = diag\left(\sqrt{\beta_1^a}e^{j\theta_1^a},...,\sqrt{\beta_k^a}e^{j\theta_k^a},...,\sqrt{\beta_n^a}e^{j\theta_n^a}\right)$ denote as the reflection coefficient matrices of IRS, where $\sqrt{\beta_k^a} \in (0,1]$, $\theta_k^a \in (0,2\pi]$ denotes the amplitude and phase shift of the *k*-th IRS element.

2.2.2. IT phase

In the IT phase, the BS transmits information in the form of NOMA through the direct link and the IRS reflection link, meanwhile, Alice transmits sensing signals to Bob, and under the null hypothesis H_0 (Alice does not receive the sensing signals reflected by Bob) and the alternative hypothesis H_1 (Alice receives the sensing signals reflected by Bob), the signals received at Alice and at Bob in the IT phase are

$$y_A(t) = \begin{cases} x_{BS}(t)(h_{ra}\Theta_A h_{br} + g_{ba}) + n_a(t), & H_0 \\ x_{BS}(t)(h_{ra}\Theta_A h_{br} + g_{ba}) + f_{ab}f_{ba}\sqrt{\sigma_{rcs}P_A}x_r(t-\frac{2d}{c}) + n_a(t) & H_1 \end{cases} \tag{2}$$

$$y_B(t) = x_{BS}(t)(h_{br}\Theta_B h_{rb} + g_{bb}) + f_{ab}\sqrt{P_A}x_r(t) + n_b(t) \tag{3}$$

where $x_{BS}(t) = \sqrt{\alpha_a P_{BS}}x_a(t) + \sqrt{\alpha_b P_{BS}}x_b(t)$, α_a and α_b are power distribution coefficients of the Alice and Bob, respectively, with $\alpha_b > \alpha_a$ and $\alpha_a + \alpha_b = 1$; $x_a(t)$, $x_b(t)$ and $x_r(t)$ are the transmitted signals corresponding to $BS \to Alice$, $BS \to Bob$ and $Alice \to Bob$ with $E\left\{\left|x_a(t)\right|^2\right\} = E\left\{\left|x_b(t)\right|^2\right\} = E\left\{\left|x_r(t)\right|^2\right\} = 1$. In addition, $P_A = \frac{P_{BS}\eta\rho\left|h_{ra}\Theta_A h_{br} + h_{ba}\right|^2}{4\pi d^2(1-\rho)}$ denotes the transmit power at Alice, σ_{rcs} is the radar cross section of Bob, *d* is the range between the Alice and Bob, *c* is the speed of light, $\Theta_B = diag\left(\sqrt{\beta_1^b}e^{j\theta_1^b},...,\sqrt{\beta_k^b}e^{j\theta_k^b},...,\sqrt{\beta_m^b}e^{j\theta_m^b}\right)$ is defined the same as Θ_A. $n_a(t)$, $n_b(t)$ represents the complex additive white Gaussian noise (AWGN) which follows $n_a(t) \sim CN\left(0,\sigma_a^2\right)$, $n_b(t) \sim CN\left(0,\sigma_b^2\right)$.

As the communication signals have a higher power level compared to sensing signals, it is preferable to fix the order of SIC-based radar echo detection at the end. According to the NOMA

protocol, the signal $x_b(t)$ is decoded at Bob and $x_a(t)$ and $x_b(t)$ are decoded with SIC at Alice. the SINR at Alice and Bob can be expressed as

$$\gamma_{x_b}^{BA} = \frac{\alpha_b P_{BS} \left| h_{ra} \Theta_A h_{br} + h_{ba} \right|^2}{\alpha_a P_{BS} \left| h_{ra} \Theta_A h_{br} + h_{ba} \right|^2 + \sigma_{rcs} P_A \left| f_{ab} \right|^2 \left| f_{ba} \right|^2 + \sigma_a^2} \tag{4}$$

$$\gamma_{x_a}^{BA} = \frac{\alpha_a P_{BS} \left| h_{ra} \Theta_A h_{br} + h_{ba} \right|^2}{\sigma_{rcs} P_A \left| f_{ab} \right|^2 \left| f_{ba} \right|^2 + \sigma_a^2} \tag{5}$$

$$\gamma_{x_r}^{BA} = \frac{\sigma_{rcs} P_A \left| f_{ab} \right|^2 \left| f_{ba} \right|^2}{\sigma_a^2} \tag{6}$$

$$\gamma_{x_b}^{BB} = \frac{\alpha_b P_{BS} \left| g_{rb} \Theta_B g_{br} + g_{bb} \right|^2}{\alpha_a P_{BS} \left| g_{rb} \Theta_B g_{br} + g_{bb} \right|^2 + P_A \left| f_{ab} \right|^2 + \sigma_b^2} \tag{7}$$

3. Performance Analysis

In this section, performance metrics such as OP and PD are used for system communication and sensing performance evaluation. OP calculated to analyze the reliability of the system communication, and the evaluation of the system perceptual performance is completed by deriving PD. In addition, we study the asymptotic expression of OP diversity order under high SNR conditions and analyze JDCCP in NOMA-ISAC networks.

3.1. Outage Probability Analysis

3.1.1. Outage probability for Bob

The outage event occurs when Bob fails to successfully decode $x_b(t)$. The OP expression for Bob can be given by

$$P_{out}^{BB} = 1 - P_r\left(\gamma_{x_b}^{BB} > \gamma_{thb}\right) \tag{8}$$

where the γ_{thb} is the threshold value of SNR at the Bob.

According to \cite{222}, the CDF of $\left| h_{ra} \Theta_A h_{br} + h_{ba} \right|^2$ can be approx-imated as a complex Gaussian random variable with mean 0 and variance $K_n \lambda_{ra} \lambda_{br} + \lambda_{hba}$, i.e., $\left| h_{ra} \Theta_A h_{br} + h_{ba} \right|^2 \sim CN\left(0, K_n \lambda_{ra} \lambda_{br} + \lambda_{hba}\right)$. Same as $\left| h_{ra} \Theta_A h_{br} + h_{ba} \right|^2$, we can obtain $\left| g_{rb} \Theta_B g_{br} + g_{bb} \right|^2 \sim CN\left(0, K_m \lambda_{rb} \lambda_{br} + \lambda_{gbb}\right)$, we following derive the OP to measure the system reliability.

The analytical expressions for OP of Bob are given by

$$P_{out}^{BB} = 1 + \Delta_1 e^{\Delta_1 - \frac{\gamma_{thb} \sigma_b^2}{H_1 H_3 P_{BS}}} Ei(-\Delta_1) \tag{9}$$

where $\Delta_1 = \frac{H_1 H_3 H_4}{H_2 \lambda_{ab} \gamma_{thb} \eta \rho}$, $H_1 = K_m \lambda_{rb} \lambda_{br} + \lambda_{gbb}$, $H_2 = K_n \lambda_{ra} \lambda_{br} + \lambda_{hba}$, $H_3 = \alpha_b - \gamma_{thb} \alpha_a$,

$H_4 = 4\pi d^2(1-\rho)$.

At high SNRs, i.e, $\gamma = \frac{P_{BS}}{\sigma_b^2} \to \infty$, we can write the approximate expression for the Bob of NOMA-ISAC networks as follows:

$$P_{out,\infty}^{BB} = 1 + \Delta_1 e^{\Delta_1} Ei(-\Delta_1) \tag{10}$$

Following the asymptotic principle, in the case of high SNRs, we can simplify Eq. (9) to obtain Eq. (10).

3.1.2. Outage Probability for Alice

If Alice communicates successfully, it must be able to decode both $x_b(t)$ and $x_a(t)$. Thus, the analytic expression for OP of Alice is

$$P_{out}^{BA} = 1 - \Pr(\gamma_{x_b}^{BA} > \gamma_{thb}, \gamma_{x_a}^{BA} > \gamma_{tha}) \tag{11}$$

where the γ_{tha} is the threshold value of SNR at the Alice.

The analytical expressions for OP of Alice are given by

$$P_{out}^{BA} = 1 - \frac{\pi M_1}{N_1 \lambda_{ab} \lambda_{ba}} \sum_{i=0}^{N_1} e^{-\frac{H_4 \Delta_2 \sigma_a^2}{H_2 P_{BS}(1-\Delta_2 \Delta_3 \varepsilon_1)}} K_0\left(2\sqrt{\frac{\varepsilon_1}{\lambda_{ab}\lambda_{ba}}}\right)\sqrt{1-\delta_i^2} \tag{12}$$

where $\Delta_2 = \max\left(\frac{\gamma_{thb}}{H_3 H_4}, \frac{\gamma_{tha}}{H_4 \alpha_a}\right)$, $\Delta_3 = \sigma_{rcs}\eta\rho$, $M_1 = \frac{1}{\Delta_2\Delta_3}$, $\varepsilon_1 = \frac{M_1(\delta_i+1)}{2}$, $\delta_i = \cos\left(\frac{(2i-1)\pi}{2N_1}\right)$, N_i is the tradeoff parameter for accuracy-complexity.

At high SNRs, the asymptotic expressions for OP of Alice can be expressed as

$$P_{out,\infty}^{BA} = 1 - \frac{\pi M_1}{N_1 \lambda_{ab} \lambda_{ba}} \sum_{i=0}^{N_1} K_0\left(2\sqrt{\frac{\varepsilon_1}{\lambda_{ab}\lambda_{ba}}}\right)\sqrt{1-\delta_i^2} \tag{13}$$

Following the asymptotic principle, we can simplify Eq. (12) to obtain Eq. (13).

For further analysis, the diversity orders of the Bob and Alice are calculated, which can be expressed as

$$l = -\lim_{\gamma\to\infty} \frac{\log(P_{out,\infty})}{\log\gamma} \tag{14}$$

The diversity orders of Bob and Alice are given by

$$l_{Bob} = l_{Alice} = 0$$

From Corollary 1-3, we can see that as the transmit SNR increases, the SINR also increases. In the high SNR regions, the OP at each node converges to a non-zero constant, indicating a diversity order of zero.

3.2. Detection Probability

Using the definition $T_A = \sum_{t=1}^{M} \frac{|y_A(t)|^2}{M}$, and letting $M \to \infty$, we can express Alice's average received power as

$$T_A = \begin{cases} P_{BS} \left| h_{ra} \Theta_A h_{br} + g_{ba} \right|^2 + \sigma_a^2, & H_0 \\ P_{BS} \left| h_{ra} \Theta_A h_{br} + g_{ba} \right|^2 + P_A \sigma_{rcs} \left| f_{ab} \right|^2 \left| f_{ba} \right|^2 + \sigma_a^2, & H_1 \end{cases} \tag{15}$$

where H_0 represents Alice does not detect a target within the time slot, and H_1 represents Alice detects a target within the time slot. For a given threshold ζ, the false alarm probability P_{FA} and detection probability P_D at Alice are respectively defined as

$$P_D = P_r(T_A \geq \zeta | H_1)$$

The analytical expressions for DP of Alice are given by

$$P_D \approx \frac{\pi M_3}{2N_3} \sum_{t=0}^{N_3} e^{-\frac{H_4(\zeta - \sigma_a^2)}{H_4 + H_2 \Lambda_3 \varepsilon_3 P_{BS}}} \frac{2}{\lambda_{ab} \lambda_{ba}} K_0 \left(2\sqrt{\frac{\theta}{\lambda_{ab}\lambda_{ba}}}\right) \sqrt{1 - \delta_t^2} \tag{16}$$

where $\varepsilon_3 = \frac{M_3(\delta_t + 1)}{2}$, $\delta_t = \cos\left(\frac{(2t-1)\pi}{2N_3}\right)$.

3.3. Joint Detection and Communication Coverage Probability

We introduce the JDCCP metric as a combined metric for the extension of communication coverage and the detection probability of radar communication scenarios, the JDCCP of Alice can be expressed as

$$D\left(T_A > \zeta; \gamma_{x_b}^{BA} > \gamma_{thb}; \gamma_{x_a}^{BA} > \gamma_{tha} \middle| H_1\right) \tag{17}$$

This gives the probability of radar detection occurring for a given detection threshold, while ensuring Alicen can successfully decode its own messages to achieve the communication requirement. A threshold γ is chosen to meet the detection probability requirement, and then a JRDCCP metric is obtained for a given communication threshold θ.

4. Numerical Results

Table 1: System simulation parameter setting table.

Channel parameter	$\lambda_{br} = 0.3, \lambda_{rb} = 0.3, \lambda_{gbb} = 0.5, \lambda_{ra} = 0.4, \lambda_{gba} = 0.2, \lambda_{ab} = \lambda_{ba} = 0.1$
Power distribution factor	$\alpha_b = 0.8, \alpha_a = 0.2$
The distance between Alice and Bob	$d = 10m$
Time switching factor	$\rho = 0.3$
Energy conversion efficiency	$\eta = 0.8$
Number of IRS elements	$K = K_n = K_m = 64$
Radar cross-sectional area	$\sigma_{RCS}^B = 20dB$

This section verifies the correctness of the theoretical analysis in Section 3 by comparing the

Monte Carlo simulation results with the theoretical analysis and evaluating the performance of the NOMA-ISAC system. In subsequent simulations, we set parameter values as shown in Table 1, unless otherwise stated.

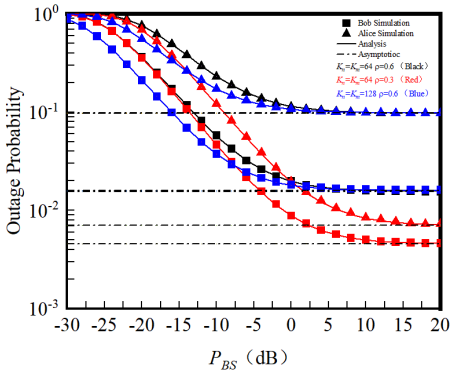

Figure 2: The variation curve of OP with transmitting power under different IRS component quantity and time allocation factor ρ.

Figure 2 shows the OPs of Bob and Alice for the NOMA-ISAC system for different numbers of IRS originals K and different P_{BS}. It can be seen that the results of the theoretical analysis match well with the Monte Carlo simulation results. As the BS transmit power increases, the OPs of Bob and Alice decrease and tend to be constant in the high SNR region, resulting in a diversity order of zero. By comparing the OPs for the same K conditions, it can be concluded that increasing P_{BS} leads to a decrease in OPs. The main reason for this is that increasing p leads to an increase in P_A power, which increases SINR and thus decreases OPs in the process of decoding the information. On the other hand, increasing K decreases the OPs in the same P_{BS} condition, but the OPs are the same in the high SNR region for K=64 and K=128. Finally, it can be concluded that increasing the number of IRS elements can effectively improve the reliability of communication.

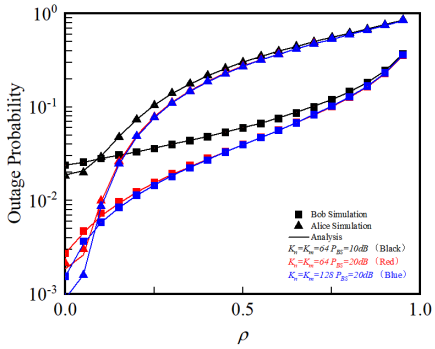

Figure 3: The change curve of OP with ρ under different IRS element quantity and transmitting power.

Figure 3 shows the variation in OPs with $\boldsymbol{\rho}$ for the NOMA-ISAC system. We set P_{BS}=10 dB and 20 dB. From the simulation results, we can see that the OPs of Alice and Bob increase with increasing $\boldsymbol{\rho}$. This is due to the fact that increasing $\boldsymbol{\rho}$ increases the transmission power of the P_A, which decreases the SINR of Alice and Bob, leading to an increase in OPs. Comparing the OPs for the same K condition, we can see that increasing the BS transmit power decreases the OPs, and comparing the OPs for different K conditions, we can conclude that increasing K decreases the OPs for Alice and Bob, and converges for $\boldsymbol{\rho}$ greater than 0.5. Therefore, we can conclude that the improvement of the reliability of the communication system is better achieved by increasing the

transmit power of the BS.

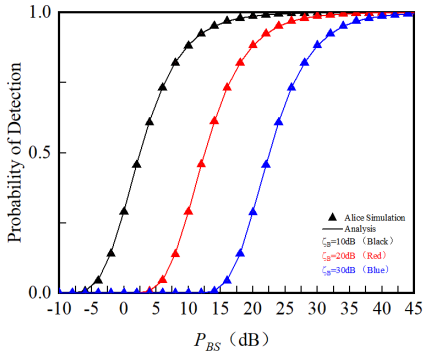

Figure 4: PD change curve with transmitted power under different detection thresholds

The DP of Alice versus BS transmit power for different detection thresholds is shown in Figure 4. Intuitively, the DP can be increased by increasing the BS transmit power. This is due to the fact that an increase in the BS transmit power leads to an increase in the power of Alice's received signal and a consequent increase in Alice's DP for a determined detection threshold. On the other hand, as the detection threshold increases, a larger P_{BS} is required to achieve the same detection probability. Therefore, in the current system design, a reasonable allocation of power should be made according to the different needs of sensing and communication.

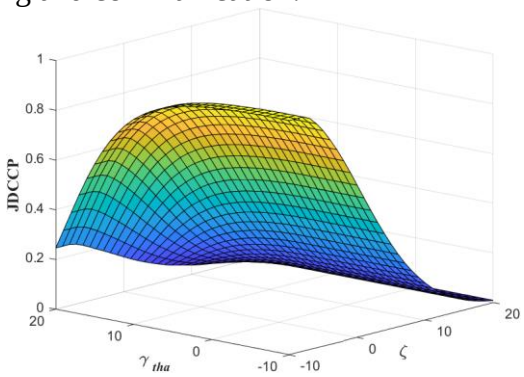

Figure 5: JDCCP 3D diagram.

Figure 5 illustrates the relationship between JDCCP and different γ_{tha} and ζ, given $\gamma_{thb} = 0.6$. For lower values of ζ, the detection probability approaches 1 and the JDCCP metric converges to the communication coverage probability. Conversely, when the communication threshold of Alice γ_{tha} is in the lower range, the communication coverage probability approaches 1 and the JDCCP metric tends to equal the detection probability.

5. Conclusion

In this paper, we propose a novel NOMA-ISAC framework that combines the advantages of IRS and energy harvesting techniques. Based on this, we investigate the OP and ER of the IRS-assisted NOMA-ISAC network based on the energy harvesting strategy, and derive relevant analytical expressions for both, and obtain asymptotic expressions for the OP in the high SNR region. For the evaluation of the sensing performance, we derived the DP expression for the detection vehicle and introduced the JRDCCP metric to realize the joint evaluation of the communication performance and the sensing performance. The numerical results given verify the accuracy of the derived

expressions and show that the trade-off between communication and perceptual performance can be achieved by adjusting various parameters of the system under consideration. In addition, we analyze the effects of different factors on system performance by adjusting other parameters.

References

[1] Saad W, Bennis M, Chen M. A vision of 6G wireless systems: Applications, trends, technologies, and open research problems [J]. IEEE network, 2019, 34(3): 134-142.

[2] De Lima C, Belot D, Berkvens R, et al. Convergent communication, sensing and localization in 6G systems: An overview of technologies, opportunities and challenges[J]. IEEE Access, 2021, 9: 26902-26925.

[3] Zhang J A, Liu F, Masouros C, et al. An overview of signal processing techniques for joint communication and radar sensing [J]. IEEE Journal of Selected Topics in Signal Processing, 2021, 15(6): 1295-1315.

[4] Zhang J A, Rahman M L, Wu K, et al. Enabling joint communication and radar sensing in mobile networks—A survey[J]. IEEE Communications Surveys & Tutorials, 2021, 24(1): 306-345.

[5] Liu A, Huang Z, Li M, et al. A survey on fundamental limits of integrated sensing and communication[J]. IEEE Communications Surveys & Tutorials, 2022, 24(2): 994-1034.

[6] Mu J, Gong Y, Zhang F, et al. Integrated sensing and communication-enabled predictive beamforming with deep learning in vehicular networks[J]. IEEE Communications Letters, 2021, 25(10): 3301-3304.

[7] Wang X, Fei Z, Huang J, et al. Joint waveform and discrete phase shift design for RIS-assisted integrated sensing and communication system under Cramer-Rao bound constraint[J]. IEEE Transactions on Vehicular Technology, 2021, 71(1): 1004-1009.

[8] Wang Z, Liu Y, Mu X, et al. NOMA empowered integrated sensing and communication[J]. IEEE Communications Letters, 2022, 26(3): 677-681.

[9] Wang Z, Liu Y, Mu X, et al. NOMA inspired interference cancellation for integrated sensing and communication [C]//ICC 2022-IEEE International Conference on Communications. IEEE, 2022: 3154-3159.

[10] Li X, Zhao M, Zeng M, et al. Hardware impaired ambient backscatter NOMA systems: Reliability and security[J]. IEEE Transactions on Communications, 2021, 69(4): 2723-2736.

[11] Liu X, Zhai X B, Lu W, et al. QoS-guarantee resource allocation for multibeam satellite industrial internet of things with NOMA[J]. IEEE Transactions on Industrial Informatics, 2019, 17(3): 2052-2061.

[12] Memisoglu E, Türkmen H, Ozbakis B A, et al. CSI-based NOMA for Integrated Sensing and Communication[J]. IEEE Wireless Communications Letters, 2023.

[13] Ouyang C, Liu Y, Yang H. On the performance of uplink ISAC systems[J]. IEEE Communications Letters, 2022, 26(8): 1769-1773.

[14] Tao L, Yang W, Lu X, et al. Achieving covert communication in uplink NOMA systems via energy harvesting jammer[J]. IEEE Communications Letters, 2021, 25(12): 3785-3789.

[15] Pham Q V, Fang F, Ha V N, et al. A survey of multi-access edge computing in 5G and beyond: Fundamentals, technology integration, and state-of-the-art [J]. IEEE access, 2020, 8: 116974-117017.

[16] Xia S, Yao Z, Li Y, et al. Online distributed offloading and computing resource management with energy harvesting for heterogeneous MEC-enabled IoT[J]. IEEE Transactions on Wireless Communications, 2021, 20(10): 6743-6757.

[17] Do D T, Le A T, Liu Y, et al. User grouping and energy harvesting in UAV-NOMA system with AF/DF relaying[J]. IEEE Transactions on Vehicular Technology, 2021, 70(11): 11855-11868.

[18] Zargari S, Khalili A, Wu Q, et al. Max-min fair energy-efficient beamforming design for intelligent reflecting surface-aided SWIPT systems with non-linear energy harvesting model[J]. IEEE Transactions on Vehicular Technology, 2021, 70(6): 5848-5864.

[19] Liu Z, Zhao S, Wu Q, et al. Joint trajectory design and resource allocation for IRS-assisted UAV communications with wireless energy harvesting[J]. IEEE Communications Letters, 2021, 26(2): 404-408.

[20] Liu X, Zhang H, Long K, et al. Proximal policy optimization-based transmit beamforming and phase-shift design in an IRS-aided ISAC system for the THz band[J]. IEEE Journal on Selected Areas in Communications, 2022, 40(7): 2056-2069.

[21] Yang Z, Xu P, Chen G, et al. Performance analysis of IRS-assisted NOMA networks with randomly deployed users [J]. IEEE systems journal, 2022.

[22] Lyu B, Ramezani P, Hoang D T, et al. IRS-assisted downlink and uplink NOMA in wireless powered communication networks [J]. IEEE Transactions on Vehicular Technology, 2021, 71(1): 1083-1088.